INTERFACE FOCUS

royalsocietypublishing.org/journal/rsfs

Research

Cite this article: Martinez-Navarro H, Zhou X, Bueno-Orovio A, Rodriguez B. 2021 Electrophysiological and anatomical factors determine arrhythmic risk in acute myocardial ischaemia and its modulation by sodium current availability. *Interface Focus* **11**: 20190124.
http://dx.doi.org/10.1098/rsfs.2019.0124

Accepted: 23 September 2020

One contribution of 11 to a theme issue 'Computational biomedicine. Part II: organs and systems'.

Subject Areas:
biomedical engineering, computational biology, biophysics

Keywords:
myocardial ischaemia, coronary artery disease, anti-arrhythmic drugs, sodium block, Brugada syndrome, computer simulations

Author for correspondence:
Blanca Rodriguez
e-mail: blanca.rodriguez@cs.ox.ac.uk

Electronic supplementary material is available online at https://doi.org/10.6084/m9.figshare.c.5222605.

THE ROYAL SOCIETY PUBLISHING

Electrophysiological and anatomical factors determine arrhythmic risk in acute myocardial ischaemia and its modulation by sodium current availability

Hector Martinez-Navarro, Xin Zhou, Alfonso Bueno-Orovio and Blanca Rodriguez

Department of Computer Science, British Heart Foundation Centre of Research Excellence, University of Oxford, Parks Road, Oxford OX1 3QD, UK

HM-N, 0000-0003-0234-2605; XZ, 0000-0003-2814-3399; AB-O, 0000-0002-1634-3601; BR, 0000-0002-3435-7388

Acute myocardial ischaemia caused by coronary artery disease is one of the main causes of sudden cardiac death. Even though sodium current blockers are used as anti-arrhythmic drugs, decreased sodium current availability, also caused by mutations, has been shown to increase arrhythmic risk in ischaemic patients. The mechanisms are still unclear. Our goal is to exploit perfect control and data transparency of over 300 high-performance computing simulations to investigate arrhythmia mechanisms in acute myocardial ischaemia with variable sodium current availability. The human anatomically based torso-biventricular electrophysiological model used includes representation of realistic ventricular anatomy and fibre architecture, as well as ionic to electrocardiographic properties. Simulations show that reduced sodium current availability increased arrhythmic risk in acute regional ischaemia due to both electrophysiological (increased dispersion of refractoriness across the ischaemic border zone) and anatomical factors (conduction block from the thin right ventricle to thick left ventricle). The asymmetric ventricular anatomy caused high arrhythmic risk specifically for ectopic stimuli originating from the right ventricle and ventricular base. Increased sodium current availability was ineffective in reducing arrhythmic risk for septo-basal ectopic excitation. Human-based multiscale modelling and simulations reveal key electrophysiological and anatomical factors determining arrhythmic risk in acute ischaemia with variable sodium current availability.

1. Introduction

Acute myocardial ischaemia is a leading cause of sudden cardiac death, produced by reduced blood flow in the coronary arteries. Its causes include blood clot formation, atherosclerosis or vasospasm and its electrophysiological consequences increase the risk of lethal arrhythmias such as ventricular fibrillation. The risk is particularly high in the early phase of acute ischaemia (first 10–15 min post-occlusion) [1]. The occurrence of ischaemia-induced arrhythmias is also modulated by additional conditions, such as drug-induced effects and channelopathies. Thus, as reported in the clinical trial CAST (Cardiac Arrhythmia Suppression Trial), sodium channel blockers may increase arrhythmic risk in patients suffering from recurrent acute ischaemia episodes [2,3]. Furthermore, studies have highlighted the genetic predisposition to ischaemia-induced arrhythmias of patients with sodium current (I_{Na}) channelopathies, such as Brugada syndrome or Lenègre's disease [4,5].

Huge advances in technologies and credibility of multiscale biophysical modelling and simulation have opened new avenues for the *in silico* evaluation

of therapies and clinical conditions [6–10]. The multiscale nature of modelling and simulation allows unravelling underlying mechanisms from subcellular processes (such as ionic currents) to whole organ dynamics (such as reentrant arrhythmias) and the electrocardiogram. These techniques have been used to investigate the electrophysiological consequences of acute regional ischaemia on the ECG and arrhythmic risk, demonstrating excellent agreement with experimental and clinical recordings, as shown in [11–13]. Moreover, previous studies have shown the role of I_{Na} alterations caused by drugs and mutations in modulating arrhythmic risk in the human ventricles [14,15]. However, the interplay between acute ischaemia and I_{Na} availability in determining arrhythmia mechanisms is still unclear.

The aim of this study is to investigate the mechanisms of modulation of arrhythmic risk caused by altered I_{Na} availability in the human ventricles affected by the electrophysiological alterations caused by acute regional ischaemia. We hypothesize that both electrophysiological and anatomical factors determine the establishment of reentrant circuits in acute regional ischaemia and their modulation by I_{Na} availability.

2. Methods

2.1. Human torso-biventricular multiscale model of electrophysiology in acute regional ischaemia

The human biventricular model embedded in a torso, constructed and evaluated in our previous study [12] was used to simulate the concomitant effect of acute regional ischaemia and changes in sodium current availability from ionic dynamics to body surface potentials. In this study, the transmural ischaemia caused by LAD occlusion was selected in the simulations, since it was the most pro-arrhythmic case in [12]. The 12-lead ECG signal was computed from standard clinical lead positions on the torso. Details on the modelling and simulation framework and its validation are presented in [12].

In brief, human membrane kinetics were represented with the modified version of the O'Hara–Rudy (ORd) model [16] proposed by Dutta *et al*. [17] to overcome the limitations of the original model in reproducing electrical conduction and refractoriness under ischaemic conditions. Acute ischaemia was simulated in its early phase, before gap junctional uncoupling takes place, corresponding to high arrhythmic risk during the first 10–15 min post-occlusion, as indicated by experimental studies in animals [1,18]. Acquiring evidence on regional ischaemia-induced arrhythmia susceptibility in human would be challenging as most episodes occur out-of-hospital, and experimental ischaemia induction is constrained by ethical and also technical limitations (see also [19]). The ischaemic region was modelled as in [12,20], including (i) the ischaemic core zone (ICZ); (ii) the lateral border zone (BZ); and (iii) the endocardial BZ [21–23]. Ionic changes derived from the main electrophysiological effects of acute ischaemia (hyperkalemia, hypoxia and acidosis) were introduced in ischaemic tissue using values from experimental findings [21,23–25]. Hyperkalaemia led to an increased extracellular potassium concentration ($[K^+]_o = 9.5$ mmol l^{-1}); hypoxia enabled an ATP-dependent K^+ current ($I_{K(ATP)}$) by applying a scaling factor of 0.07 (0.00 if non-ischaemic) to the peak conductance of the current, estimated in 0.05 mS μF^{-1} [26]; and acidosis caused a decreased peak conductance of I_{Na} and L-type calcium currents (I_{CaL}) by 25%. The BZ was modelled providing a linear transition in ischaemic parameters between the ICZ and the normal zone (NZ) tissue, as shown experimentally [22,23] and computationally [12,20,27–30]. NZ tissue had a $[K^+]_o$ of 5.4 mmol l^{-1} (baseline value in the ORd model), zero $I_{K(ATP)}$ and default conductances for I_{Na} and the L-type calcium current as in the ORd model.

The bidomain equations were used to describe electrical conduction in the ventricular and torso domains and were discretized in space using a volumetric tetrahedral mesh, and solved with the finite-element method in CHASTE [31,32]. The spatial discretization of the myocardium was averagely 0.4 mm between nodes, which guaranteed numerical convergence [20,33]. The total volumetric mesh is based on 2.51 million nodes and 14.2 million tetrahedral elements.

Fibre orientation was imposed in the myocardial mesh with a rule-based method that reproduces the experimental findings by Streeter *et al*. [34]. Transmural and apico-basal electrophysiological heterogeneities were implemented in the myocardial model as described in [12] to reproduce experimental findings in healthy control conditions [35,36].

2.2. Stimulation protocols and quantification of the inducibility of arrhythmias

To simulate sinus rhythm, a realistic activation sequence [37] was implemented as described in [33], based on a fast conduction system mimicking propagation through the subendocardial Purkinje network at a propagation speed of 140 cm s^{-1}. This yielded realistic QRS complexes in the 12-lead ECG. Four endocardial regular stimuli (S1) were applied with a cycle length of 1000 ms. Simulated ECGs and activation sequences were stabilized after the first two S1 stimuli, with the third and fourth stimuli producing consistent results. To evaluate reentry vulnerability, an additional ectopic stimulus (S2) was applied transmurally. This was based on the experimental evidence from [38] showing that the earliest activity of premature stimuli in acute myocardial ischaemia was identified in the normal myocardium adjacent to the ischaemic region, and that no important time differences were found between endo- and epicardium. The vulnerability window for reentry (VW) was defined as the range of coupling intervals (CI, i.e. time difference between the last S1 and S2) [6,28,39] which induced reentrant arrhythmias, as used previously for quantification of arrhythmic risk in whole-ventricular simulation studies [12,14,20]. Six different ectopic S2 locations were considered for each scenario, equally spaced around the ischemic BZ (in agreement with the location of ectopy in ischaemia experiments [22,38]). For each case, the simulated electrical activation pattern was analysed to identify the formation of reentrant circuits. In total, more than 400 simulations of 5–15 h each on 720 CPUs were conducted. Further details of the computational model of human ventricular electrophysiology in acute ischaemia can be found in [12].

2.3. Alterations in I_{Na} availability

In this study, we aim to analyse the effects of changes in I_{Na} availability in the formation of ischaemia-induced reentries. For this, we considered two scenarios with reduced I_{Na} availability. The first case involved a 50% reduction of the I_{Na} conductance with respect to baseline, which occurs in patients presenting SCN5A loss-of-function mutations [40]. The second scenario was a 25% reduction of the I_{Na} conductance with respect to baseline, which could represent drug-induced block. This degree of current block is estimated from a single pore block model [41], using the IC_{50} and n_H values for each drug–channel interaction extracted from [42]. We focused on the role of conductance in I_{Na} availability rather than current kinetics as considered in previous studies in healthy ventricles [15].

Clinical doses of sodium blockers vary (for example, the starting dose of flecainide is 100 mg per day, and the maximum recommended dose in 24 h is 600 mg [43,44]), resulting in

Table 1. I_{Na} block values computed for selected channel blockers at different doses: 1, 3 and 5 times the maximum effective free therapeutic plasma concentration $EFTPC_{max}$. IC_{50} and n_H values for the different pharmacological compounds are extracted from [42].

drug	IC_{50} (nM)	n_H	$EFTPC_{max}$ (nM)	ionic block at $EFTPC_{max}$ (%)	ionic block at 3× $EFTPC_{max}$ (%)	ionic block at 5× $EFTPC_{max}$ (%)
flecainide	6677	1.9	752.9	1.6	11.3	25.2
propafenone	3886	0.9	131.0	4.1	10.6	16.8
quinine	24 151	1.1	3956.7	11.8	31.2	44.5

Table 2. Measurement of electrophysiological properties under varying I_{Na} conditions, measured in one-dimensional fibres based on the O'Hara–Rudy model. APD and CV were measured under control and ischaemic conditions with the latter presented in parentheses. Refractoriness dispersion (ΔERP) was measured as the difference between refractory periods in ischaemic and healthy cells. One-dimensional fibres were stimulated with a frequency of 1 Hz.

scenario	APD (ms)	ΔERP (ms)	CV (cm s^{-1})	V_{rest} (mV)
baseline	240 (169)	50	70.6 (42.9)	−88.0 (−72.9)
50% I_{Na} block	239 (178)	330	60 (30.8)	−88.0 (−72.9)
25% I_{Na} block	241 (170)	140	66.7 (38.7)	−88.0 (−72.9)
25% I_{Na} increase	239 (167)	20	75 (48)	−88.0 (−72.8)

variable drug concentrations in the patients' blood plasma. Table 1 shows the effects of the selected drugs on the I_{Na} at different doses: 1, 3 and 5 times the maximum effective free therapeutic plasma concentration $EFTPC_{max}$. Taking into consideration dose variability and values shown in table 1, and especially flecainide, as related to the CAST, we considered 25% I_{Na} block to evaluate arrhythmic risk derived from a drug-induced I_{Na} blockage. Additionally, we also considered a 25% I_{Na} increase to evaluate the potential effect as proposed in [45]. These alterations in I_{Na} were implemented in the whole myocardium.

2.4. Quantification of electrophysiological biomarkers

Due to the high computational cost of calculating effective refractoriness period (ERP) in different regions of the ventricle using the S1S2 simulation protocol, simulations of one-dimensional fibres were conducted to quantify electrophysiological characteristics with varying I_{Na} availability under control and ischaemic conditions in the absence of whole ventricle anatomical complexity. The fibres were 2 cm long with 100 nodes, and the stimulus current was applied to the first 3% of the fibres, and conductivity was set to 2.118 mS cm^{-1} to yield a realistic baseline longitudinal conduction velocity (CV) in humans. The one-dimensional fibres were paced under an S1–S2 protocol: regular S1 stimulus was applied with a cycle length of 1000 ms for 20 beats, and then an ectopic stimulus was set at progressively shorter CIs with 10 ms of decrement. ERP was defined as the shortest CI which enabled successful conduction at the end of the fibres. Action potential duration (APD) was calculated from the central node of the fibres from the last S1 beat as the time interval from depolarization to 90% of repolarization, and CV was measured from node 20 to node 80.

3. Results

3.1. Severe I_{Na} block led to moderate reduction in myocardial conduction velocity and significant increase in refractoriness dispersion

Table 2 shows how electrophysiological biomarkers vary with alterations in I_{Na} availability both in healthy and ischaemic tissue. Changes in I_{Na} availability altered mildly APD both under healthy and ischaemic conditions (first column). Refractoriness dispersion between healthy and ischaemic tissue was significantly increased under reduced I_{Na} availability (ΔERP under baseline conditions was 50 ms and with 50% I_{Na} block was 330 ms; see second column), which is associated with a higher likelihood of arrhythmias. Increased (25%) I_{Na} led to reduced refractoriness dispersion between the healthy and the ischaemic tissue (20 ms). I_{Na} block reduced myocardial propagation (longitudinal CV at baseline conditions was 70.6 cm s^{-1}, whereas under 50% I_{Na} block conditions, longitudinal CV was 60 cm s^{-1}). Under ischaemic conditions, the CV reduction is most pronounced in the case of I_{Na} block, leading to longitudinal CV values between 30 and 40 cm s^{-1}, as shown in the third column. The resting membrane potential (V_{rest}) was substantially increased by ischaemia (from −88 to −72.9 mV) but was not altered by variability in I_{Na} availability (last column).

3.2. Different ectopic locations highlight the key role of ventricular anatomy in ischemia-induced reentrant mechanisms

Figure 1 shows the VW obtained in the regionally ischaemic ventricles with baseline I_{Na} availability, for varying the location of the ectopic stimulus. The most pro-arrhythmic ectopic location was septum/apex (case C), followed by the left ventricle (LV) (cases A and B), right-ventricular (RV) mid-wall (case D) and septum/base (case F). The different ectopic locations also led to different types of reentry, as summarized in figure 1 (bottom panel) and illustrated in figure 2.

Ectopic stimulus in the LV (figure 1, cases A–C) and RV (figure 1, cases D and E) induced the establishment of figure-of-eight reentry, which is illustrated in figure 2*a*. Following the ectopic stimulus, unidirectional conduction block occurred in the ICZ, and propagation proceeded around the BZ (400 ms), then propagated retrogradely into the ICZ (450–500 ms), and reentered into the NZ of the RV (570 ms), as reported in [12,20,22].

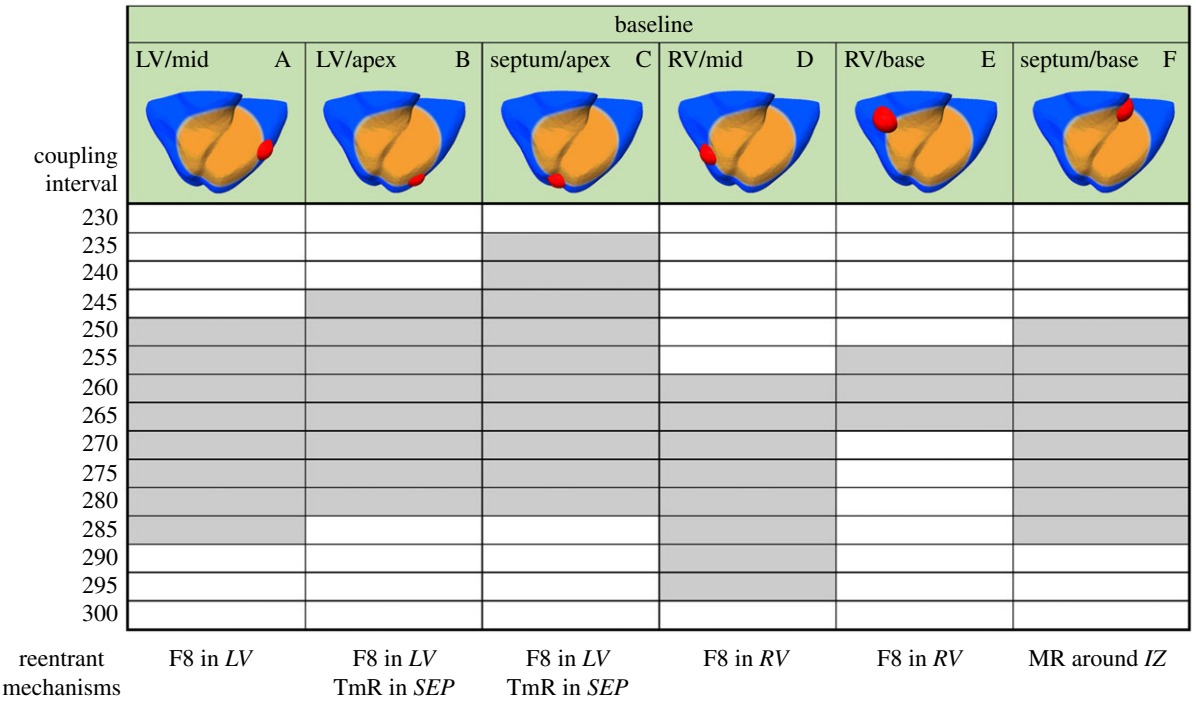

Figure 1. Vulnerability windows for reentry (grey boxes) for different locations of ectopic stimuli (red) in acute regional transmural ischaemia (orange) caused by LAD occlusion. Ectopic stimulation applied at CI = 230–300 ms at varying locations in the ischaemic border zone (cases A–F). Reentrant mechanisms observed in the vulnerability windows are annotated below. The reentry location (italic font) refers to the pathway for retrograde propagation. F8, figure-of-eight reentry; TmR, transmural micro-reentry; MR, macro-reentry; LV, left ventricle; SEP, septum; RV, right ventricle; IZ, ischaemic zone.

In addition to figure-of-eight reentry, ectopic stimuli close to the apex (cases B and C) also led to the establishment of transmural micro-reentries (figure 2*b*). As shown in Martinez-Navarro *et al*. [12], the transmural reentry was established around the ischaemic BZ in the septo-apical region. Figure 2*b* shows that the ectopic stimulus caused a bidirectional conduction block (400–570 ms) and no reentry (740 ms) on the epicardium. Nevertheless, the ectopic stimulus propagated transmurally surrounding the BZ and reentered afterwards in the healthy tissue. This established a spiral wave, anchored in the BZ in the septo-apical region (figure 2*b*(ii), 500–740 ms).

Finally, ectopic stimuli close to the base were also pro-arrhythmic as shown by the wide VW (case F), due to the establishment of macro-reentry circling around the ICZ (figure 2*c*). This type of reentry occurred following the unidirectional block at the basal region of the RV, with late activation following regular stimulation. As the RV remained refractory from the previous regular beat, the wavefront propagated towards the apex through the LV, moved around the ICZ and then reached the excitable basal region, where the reentry was completed. In summary, the location of ectopic stimulus had crucial roles in ischaemia-induced arrhythmogenesis, leading to significant differences in the vulnerability to reentry and the patterns of reentrant pathways.

3.3. Severe reduction of I_{Na} availability promotes high inducibility of reentries following ectopy in right ventricle and septum/base

Figure 3 shows the effect of 50% I_{Na} block on the VWs for the six ectopic locations considered. The results showed a large increase in the vulnerability for reentry for ectopic stimuli originated in the RV (figure 3, cases D and E) and at the base of the septum (figure 3, case F), whereas for ectopic stimulations in LV, the number of induced reentries decreased (figure 3, cases A–C). The most likely type of reentry was figure-of-eight with retrograde conduction through the LV towards the RV in cases D and E, and macro-reentry around the ICZ in case F. Ectopics in the LV and septum also led to some cases of transmural reentry (figure 3, cases B and C).

Figure 4 illustrates the mechanism explaining the larger vulnerability to reentry for ectopic stimuli located in the RV versus the LV under the condition of 50% I_{Na} block by comparing two similar scenarios: ectopic set in LV (figure 4*a*) and RV (figure 4*b*) at similar distances in the long-axis plane and at a same coupling interval of 320 ms. Both in figure 4*a*,*b*, the top area shows an epicardial view and the bottom one a slice view of the short-axis plane, with changes in the orientation to optimally illustrate the different phases of reentry.

Figure 4*a*.1 shows that the ectopic stimulus in the LV free wall propagated around the BZ, due to a conduction block in the ICZ (400–500 ms). When the wavefront surrounded the ischaemic region (570 ms), retrograde propagation (640–740 ms) towards the LV died out, and reentry failed to be established (860 ms). Figure 4*a*.2 provides a transmural view, showing following ectopic stimulation, propagation surrounded the LV cavity via the LV free wall and also through the subendocardial BZ (400 ms). Then, it progressed through the RV free wall (500–570 ms) but eventually died out as both normal and ischemic tissue were refractory (640–740 ms). Unlike figure 4*a*.1, figure 4*b*.1 displays a complete macro-reentry, starting with the stimulus propagating around the BZ (400–500 ms).

Afterwards, a slow-propagating wavefront entered the ICZ through the septum, causing retrograde propagation towards the RV (570–740 ms). Finally, the reentry is completed and sustained (860 ms). From the transmural view in figure 4*b*.2, the ectopic stimulus propagated along the RV free wall due to the

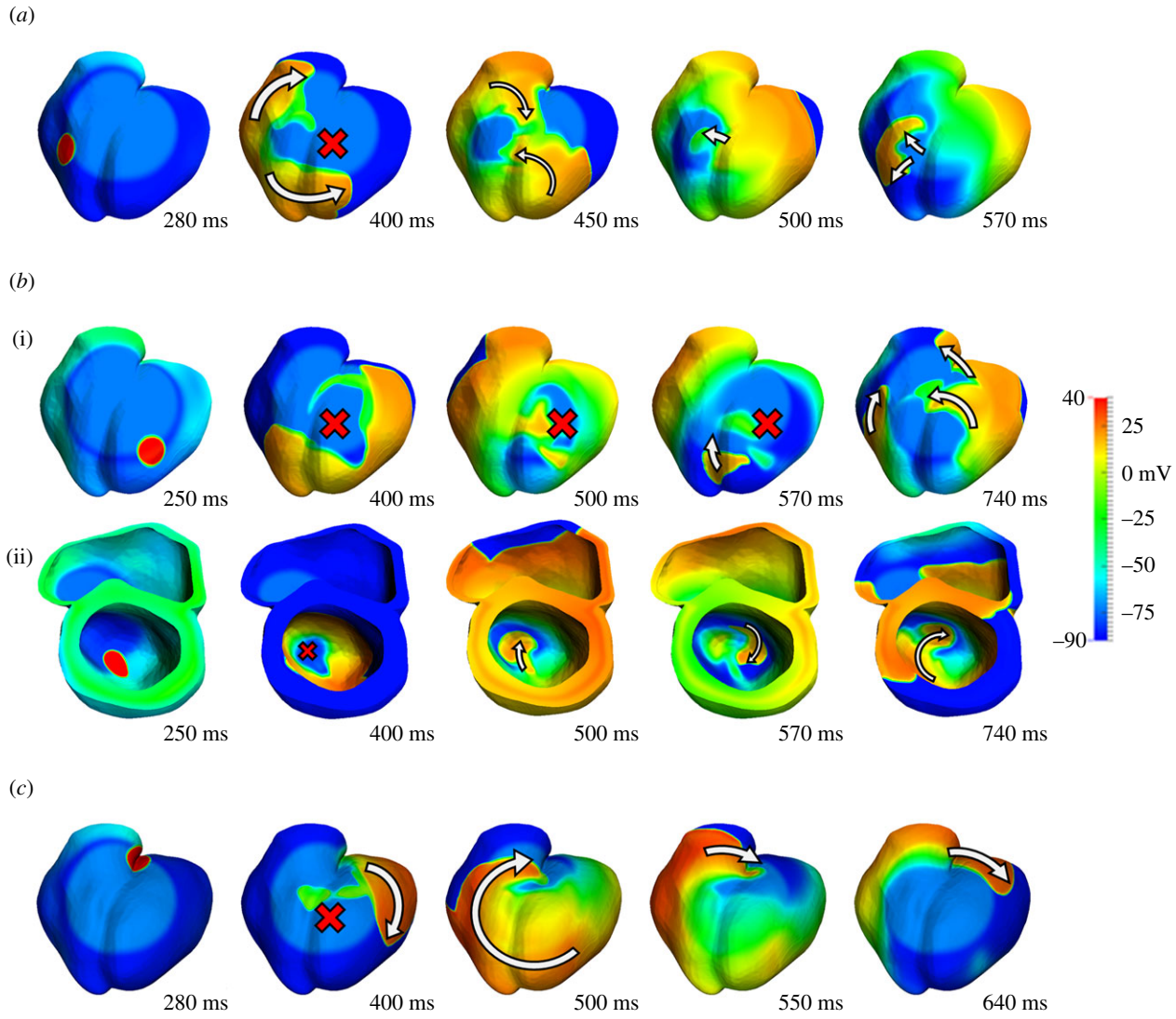

Figure 2. Main reentrant mechanisms observed in the ischaemia-induced reentry simulations. (*a*) Figure-of-eight macro-reentry, baseline ionic conditions, S2 triggered in the mid-RV at CI = 270 ms. (*b*) Transmural micro-reentry, baseline ionic conditions, S2 triggered in the LV/apex at CI = 250 ms. Epicardial (i) and septal view (ii). (*c*) Simple macro-reentry, baseline ionic conditions, S2 triggered in the septum/base at CI = 280 ms.

conduction block in the anterior ischaemic region (400 ms). Then, the wavefront propagated through the septum and LV through the inferior myocardial wall (500 ms). Depolarized tissue in the junction between the septum and LV wall eventually enabled a slow-propagating wavefront towards the thinner and excitable RV myocardial wall (570–640 ms). Once this wavefront propagated back into the healthy myocardium, the reentry was completed (740–860 ms).

The comparison between figure 4*a*,*b* proved the determining role of ventricular anatomy in modulating reentry establishment for different ectopic locations. The two ectopic S2 locations led to divergent outcomes under identical settings of ischaemic remodelling and sodium channel availability. At early stages, the activation sequence in both cases showed certain similarity (propagation of the stimulus, conduction block towards the septum and propagation across septum). The final stages were, however, very different: retrograde propagation was only possible from LV/septum to RV and not reversely. Figure 5 provides a quantification of the myocardial wall thickness in different regions. Myocardial wall thickness was measured close to the junction, with 7 and 5 mm in the septum and the LV, respectively. The RV wall was substantially thinner with a thickness of 2.4 mm, which established a substantial change in the propagation media that affected electrical conduction and promoted retrograde propagation only in the thick-to-thin direction. The LV/RV differences in wall thickness were particularly important under reduced I_{Na} conditions. Due to the remarkable increase in ΔERP induced, a major part of the ICZ remained refractory when the wavefront surrounded it. Moreover, propagation could proceed from the thick LV to the thin RV (figure 4*b*) but failed from RV to LV (figure 4*a*), due to the differences in source–sink mismatch, which were accentuated by the very low excitability present in scenarios with reduced I_{Na} and ischaemia.

3.4. Ectopic stimuli at the ventricular base are pro-arrhythmic for all degrees of I_{Na} availability tested

To further investigate the modulation of arrhythmic risk in ischaemia by I_{Na} availability, we conducted simulations considering 25% I_{Na} decrease and increase, to represent potential effects of I_{Na} block (table 1) as well as novel therapies as described in [45], respectively. Figure 6 shows VWs obtained with simulations with S2 located in the LV (figure 6*a*) and in the RV (figure 6*b*) at a similar distance from the ventricular base, and also in the septo-basal region (figure 6*c*) with progressively reduced I_{Na} availability for each stimulus location: 25% I_{Na} increase, baseline ionic conditions, 25% I_{Na} block and 50% I_{Na} block. The ectopic locations were chosen based on

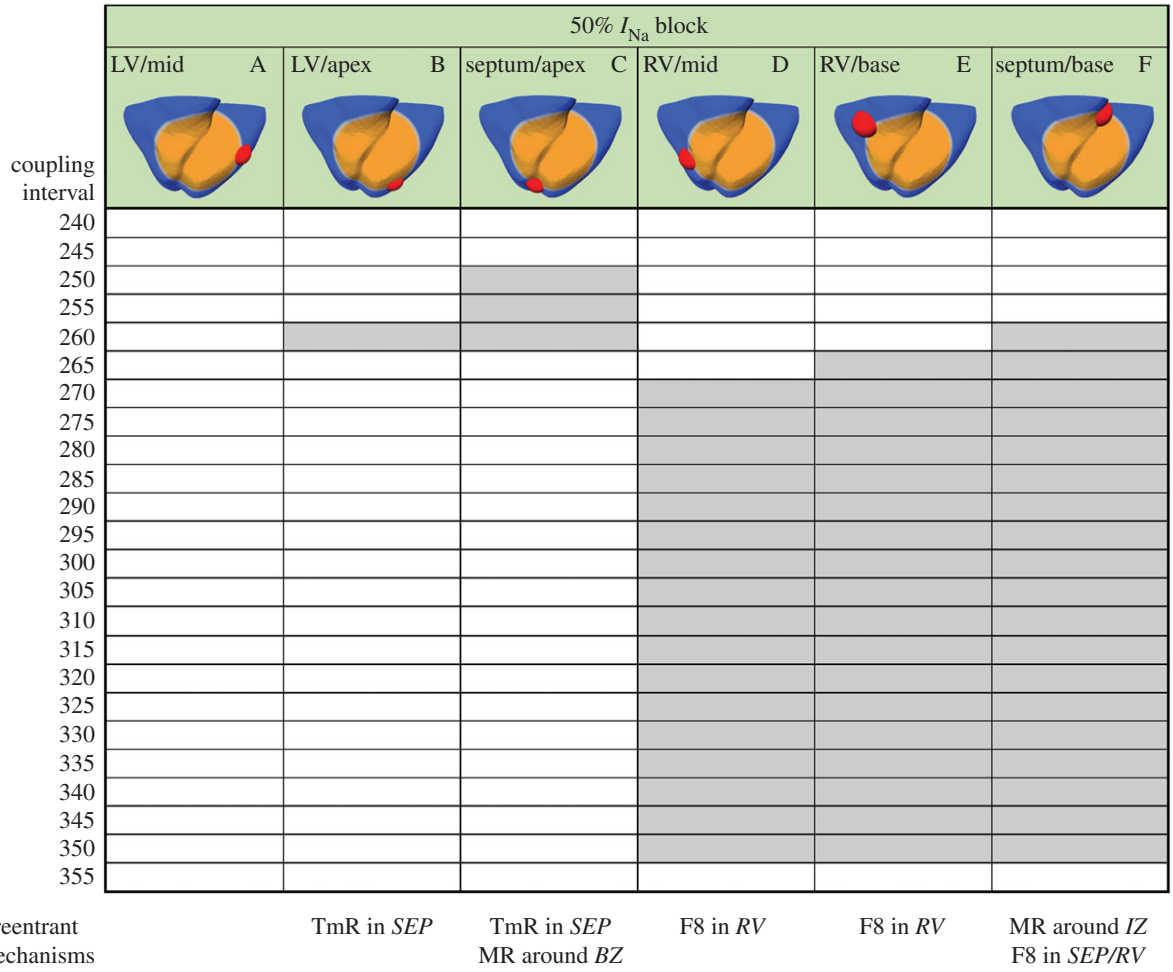

Figure 3. Vulnerability windows for reentry (grey boxes) for different locations of ectopic stimuli (red) in acute regional transmural ischaemia (orange) caused by LAD occlusion under 50% I_{Na} block. Ectopic stimulation applied at CI = 240–355 ms at varying locations in the ischaemic BZ (cases A–F). Reentrant mechanisms observed in the vulnerability windows are annotated below. The reentry location (italic font) refers to the pathway for retrograde propagation. F8, figure-of-eight reentry; TmR, transmural micro-reentry; MR, macro-reentry; LV, left ventricle; SEP, septum; RV, right ventricle; IZ, ischaemic zone.

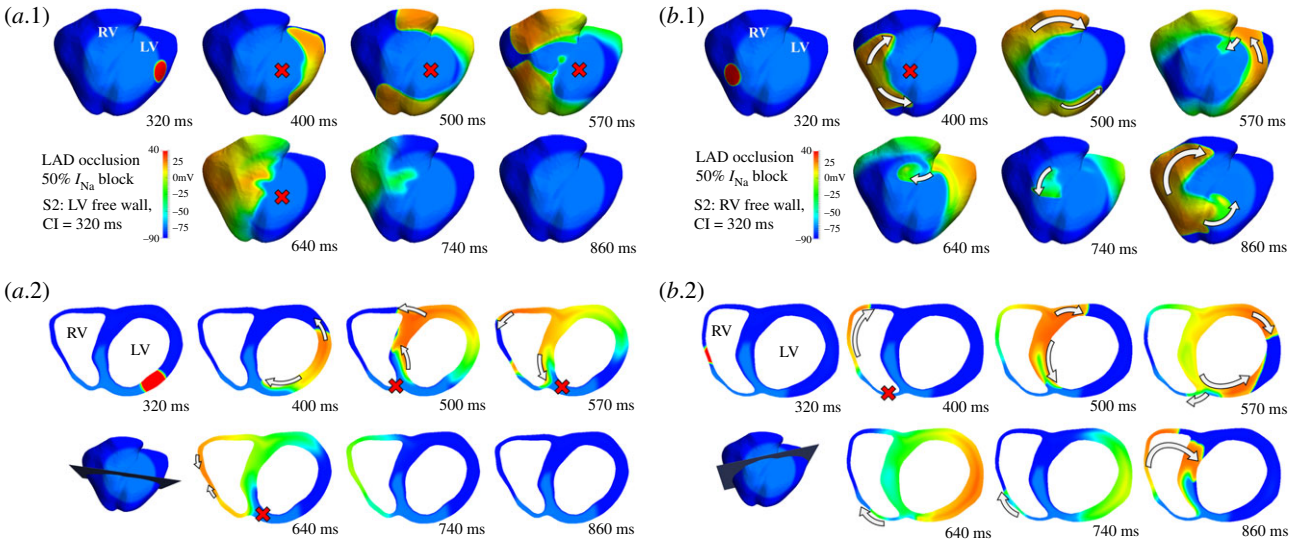

Figure 4. Comparison of activation sequences produced by ectopics set in LV and RV under 50% I_{Na} block. (*a*) Activation sequence triggered by an ectopic stimulus in the LV in simulated acute myocardial ischaemia caused by LAD occlusion with 50% I_{Na} block. (*a*.1) Epicardial view. (*a*.2) Slice visualization. No reentry was produced due to bidirectional conduction block in the anterior wall (represented by a red cross). (*b*) Activation sequence triggered by an ectopic stimulus in the RV in simulated acute myocardial ischaemia caused by LAD occlusion with 50% I_{Na} block. (*b*.1) Epicardial view. (*b*.2) Slice visualization. Unlike the stimulus originated in LV, the ectopic stimulus in the RV caused reentry based on unidirectional conduction block (400–500 ms, red cross), and posterior reentry to the RV (570–740 ms) leading to propagation towards septum and LV (860 ms).

the high occurrence of reentries observed in the base and RV (figure 3, cases D and F), and to allow the comparison between RV and LV ectopy.

As shown in the previous section, 50% I_{Na} block (figure 6, right column in each VW table) caused very large VWs (85–95 ms), unless the S2 stimulus was located in the LV

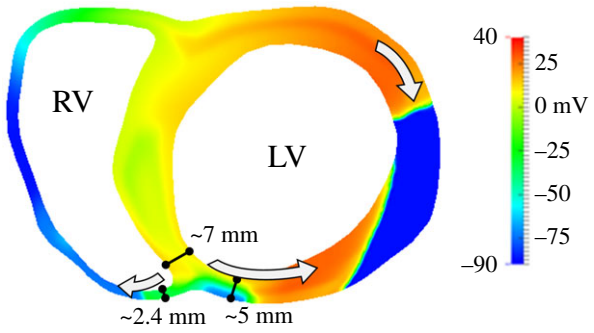

Figure 5. Quantification of myocardial wall width annotated over the activation maps at timestamp 570 ms from figure 4*b* (S2 in the RV). Note that the thick-to-thin transition promotes retrograde propagation towards the RV leading to the completion of the reentry (figure 4*b*, 860 ms).

(VW = 0 ms), in which case the bidirectional conduction block hindered the formation of reentries, due to the differences in ventricular thickness between RV and LV, as explained above.

The 25% I_{Na} block promoted the formation of figure-of-eight macro-reentries caused by stimuli triggered in the LV or RV (figure 6*a*,*b*, third column), with the VWs 15–20 ms larger compared with baseline ischaemic conditions. However, if the ectopic stimulus was set in the base (figure 6*c*, third column), the VW was similar to that in baseline conditions (40–45 ms).

Previous research suggested that increasing I_{Na} availability [45] could be an effective anti-arrhythmic therapy, and our simulations also showed that 25% increase of I_{Na} reduced the electrophysiological ERP dispersion caused by ischaemia (table 2). For 25% increase in I_{Na} availability, VWs were smaller (LV: 5 ms, RV: 10 ms) than in baseline (LV: 40 ms, RV: 15 ms) for LV and RV ectopic locations (figure 6*a*,*b*, first column). Finally, ectopics at the base led to similar VW as in baseline conditions (40 ms), as illustrated in figure 6*c* (first column).

3.5. ECG changes caused by acute ischaemia and changes in I_{Na} availability

Figure 7 shows the simulated ECG computed for healthy control conditions and baseline I_{Na} (black dashed line) and transmural ischaemia from LAD occlusion, both in baseline I_{Na} conditions (light blue solid line) and 50% I_{Na} block (dark blue solid line). As evaluated in [12], ST elevation values obtained in simulated transmural ischaemia in baseline I_{Na} conditions (light blue solid line, 274–319 µV, leads V2, V3 and V4) are within the range obtained clinically during coronary balloon LAD occlusion (200 to 500 µV in leads V2, V3 and V4) [46]. Simulated 50% I_{Na} block in acute regional ischaemia (dark blue solid line) leads to minor ECG changes, including a very mild change in QRS morphology (III, aVL, V4) or width (I, V5, V6). The ECG changes do not reflect the changes in arrhythmic risk with altered I_{Na} current availability and the key role of ectopic location in its modulation explained in the previous sections.

4. Discussion

In our study, extensive human-based computer simulations reveal the important role of both electrophysiological and anatomical factors in the modulation of pro-arrhythmic reentrant activity by I_{Na} availability in acute regional ischaemia. For low I_{Na} availability, the asymmetry of the biventricular anatomy, and specifically the differences in thickness between RV and LV, play a critical role in explaining increased arrhythmic risk in acute ischaemia. These anatomical differences explain why ectopics originating from the RV and the basal region are very prone to cause reentry for reduced I_{Na} availability. Conversely, ectopic stimuli originating from the LV often fail to propagate from the thin RV back to the thick LV hindering the establishment of reentry. Furthermore, stimuli propagating from the basal region are highly arrhythmogenic, regardless of whether the I_{Na} is blocked or enhanced. The high arrhythmic risk induced by I_{Na} block did not correlate with the very minor changes it produced on the ECG. Thus, anatomical ventricular features as well as location of ectopic stimulus and ischaemic provide a more accurate prediction of arrhythmic risk than the analysis of ECG biomarkers.

Although sodium blockers are commonly used to treat certain cardiac arrhythmias, such as atrial fibrillation [43], their use is not recommended for patients under ischaemic risk, as evidenced by the CAST [47]. The results shown in this study provide explanations on the increased arrhythmic risk resulting from sodium block when coexisting with acute myocardial ischaemia. This aligns with the increased mortality observed in those CAST patients with recurrent acute ischaemia episodes produced by a reduced and uninterrupted coronary blood irrigation [2,3]. Previous studies have also shown increased arrhythmic risk in patients with reduced I_{Na} availability, especially under ischaemic conditions [4,5]. In addition to the electrophysiological abnormalities caused by sodium block (including slow conduction and increased dispersion of refractoriness), our simulations show that arrhythmogenesis under low I_{Na} availability was drastically influenced by the available anatomical pathways that cause reentry, which are linked to the location of the ectopic stimuli. The level of I_{Na} channel availability in the normal and ischaemic areas would be expected to vary significantly between individuals and ischaemic episodes. This would translate into differences in dispersion of refractoriness and arrhythmic risk, through the mechanisms unravelled in our simulations.

In simulations considering sodium block, ectopies in the RV were more prone to induce reentrant circuits than those in the LV due to differences in ventricular thickness and hence sink–source mismatch [48,49]. This is consistent with studies stating that conduction blocks are produced in the surface area with the steepest thin-to-thick transition [50,51]. Furthermore, a simulation study on non-ischaemic ventricles [14] identified source–sink mismatch under conditions of low I_{Na} availability as a potent substrate for sustained arrhythmia caused by ectopics triggered close to regions of wall expansion. In agreement with our simulations in ischaemic conditions, Boyle *et al.* identified the septum–RV intersection as the most prone region to cause conduction block, due to source–sink mismatch potentially leading to sustained reentries. Subsequently, the authors identified the right-ventricular outflow tract (RVOT) and the posteroinferior septal region of the RV as the most pro-arrhythmic ectopic locations. These results are fully consistent with our findings: (i) the simulations of low I_{Na} availability presented in this study identified a higher occurrence of reentries than in [14], which can be explained by the presence of acute myocardial ischaemia in the anterior myocardial wall; (ii) our results also identified

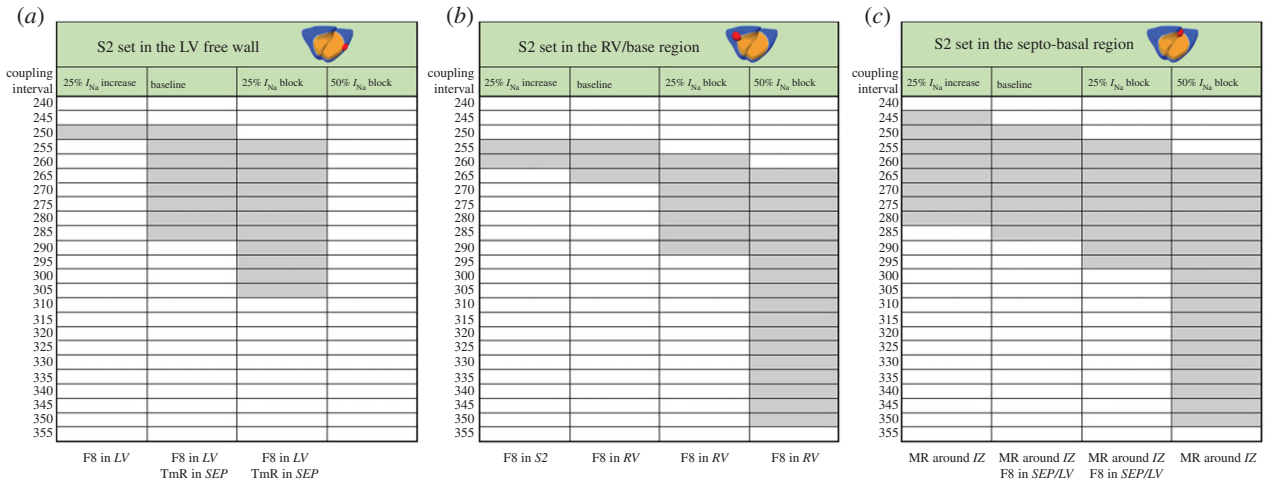

Figure 6. Vulnerability windows for reentry (grey boxes) for different locations of ectopic stimulus in acute regional transmural ischaemia caused by LAD occlusion with diverse I_{Na} availability. Ectopic stimulus applied at CI = 240–355 ms at three S2 locations: LV free wall (*a*), RV base (*b*) and septo-basal region (*c*). Reentrant mechanisms observed in the vulnerability windows are annotated (bottom). The reentry location (italic font) refers to the pathway for retrograde propagation. Each S2 location triggered certain types of reentry and varying I_{Na} availability affected the occurrence of these reentrant pathways. F8, figure-of-eight reentry; TmR, transmural micro-reentry; MR, macro-reentry; LV, left ventricle; SEP, septum; RV, right ventricle; IZ, ischaemic zone.

the septal insertion region as crucial in the establishment of reentries; and (iii) although the ectopic locations in this study are not identical to those in Boyle's work, in both studies, the ectopics triggered in the basal and septal regions of the RV are the most prone to induce reentries.

In our study, stimuli originating from the septo-basal region caused the largest VWs, characterizing them not only as highly pro-arrhythmic, but also leading to robust reentrant circuits not affected by I_{Na} availability. These observations are consistent with previous clinical reports: the free-wall region of the RVOT has been identified as the most common origin of premature stimuli in Brugada patients [52], while Morita *et al*. [53] identified ectopics in that region as the most prone sites to induce ventricular fibrillation among Brugada patients. Note that in the reentries produced by septo-basal ectopic stimuli, retrograde propagation takes place from LV to RV, as seen in reentries caused by RV stimuli. Our simulation results demonstrated that the wider VWs caused by RV/basal ectopics were explained by mechanisms highlighting the interventricular differences in wall thickness as critical factors.

As discussed, severe I_{Na} block increased drastically arrhythmic risk under ischaemic conditions, in spite of very minor changes exhibited in the ECG (figure 7). Increased vulnerability to reentry could be explained by the very pronounced increase in dispersion in refractory period and yet moderate decrease in CV caused by I_{Na} block (table 2). However, I_{Na} block caused negligible ECG changes as previously reported in clinical studies, such as [54]. Our simulations highlight the fact that anatomical factors such as the location of the ischaemic region intersecting the antero-septal region [12] as well as the location of the premature ectopic stimulus in the RV or the base, as shown in this study, are critical factors for arrhythmic risk in acute ischaemia.

According to our simulations, increasing I_{Na} availability does not guarantee an effective anti-arrhythmic strategy for patients with unifocal ectopies originating from the basal region of the myocardium or adjacent area, as this reentrant pathway was relatively robust against the changes in I_{Na} availability. Increasing I_{Na} availability produced an anti-arrhythmic reduction in dispersion of refractoriness, mostly due to ERP shortening in the ischaemic tissue to values closer to the ones in the normal tissue. Therefore, its benefits very much rely on the intervention reaching the ischaemic tissue. However, short ERP in myocardial tissue allows a fast electrical recovery that provides instability to the myocardial activation sequence, as reported in [55–57]. Moreover, I_{Na} availability could be correlated to the occurrence of ectopic beats, as hypothesized in [47]. Therefore, a higher I_{Na} availability could lead to unwanted side effects, such as a higher occurrence of ectopic beats based on the increased excitability in the myocardial tissue. Our results suggest that increasing I_{Na} showed to be only partially effective as an anti-arrhythmic strategy for patients under ischaemic risk, given that the increase in I_{Na} could be ineffective in reducing ischaemia-induced arrhythmic risk for ectopic stimulation in the base. We propose our computational pipeline to investigate the safety and efficacy of other potential anti-arrhythmic strategies including therapy or drug-induced multi-channel block.

4.1. Limitations

The effects of sodium channel blockers are not limited to reducing the I_{Na} conductance, as it also affects the sodium channel kinetics [15]. Apart from reduced I_{Na} availability, Brugada syndrome patients suffer also heterogeneities in the RVOT (either in depolarization, repolarization or a combination of both) [58–60], or abnormal recovery from inactivation in specific SCN5A variants [61–63], to cite some, which were not considered in this study. However, decreased I_{Na} functionality is an important factor of these pathologies, and here we focused on isolating its modulation of arrhythmic risk under concurring acute regional ischaemia. Exploring the sensitivity to small variations in the S2 location represents a difficulty due to the high computational cost of the simulations.

5. Conclusion

Multiscale simulations using a human biventricular ventricular model show that anatomical factors as well as electrophysiological properties explain increased arrhythmic risk in acute ischaemia caused by changes in I_{Na} availability. Our results provide a mechanistic explanation for clinical studies identifying the RVOT as the most pro-arrhythmic ectopic location, for

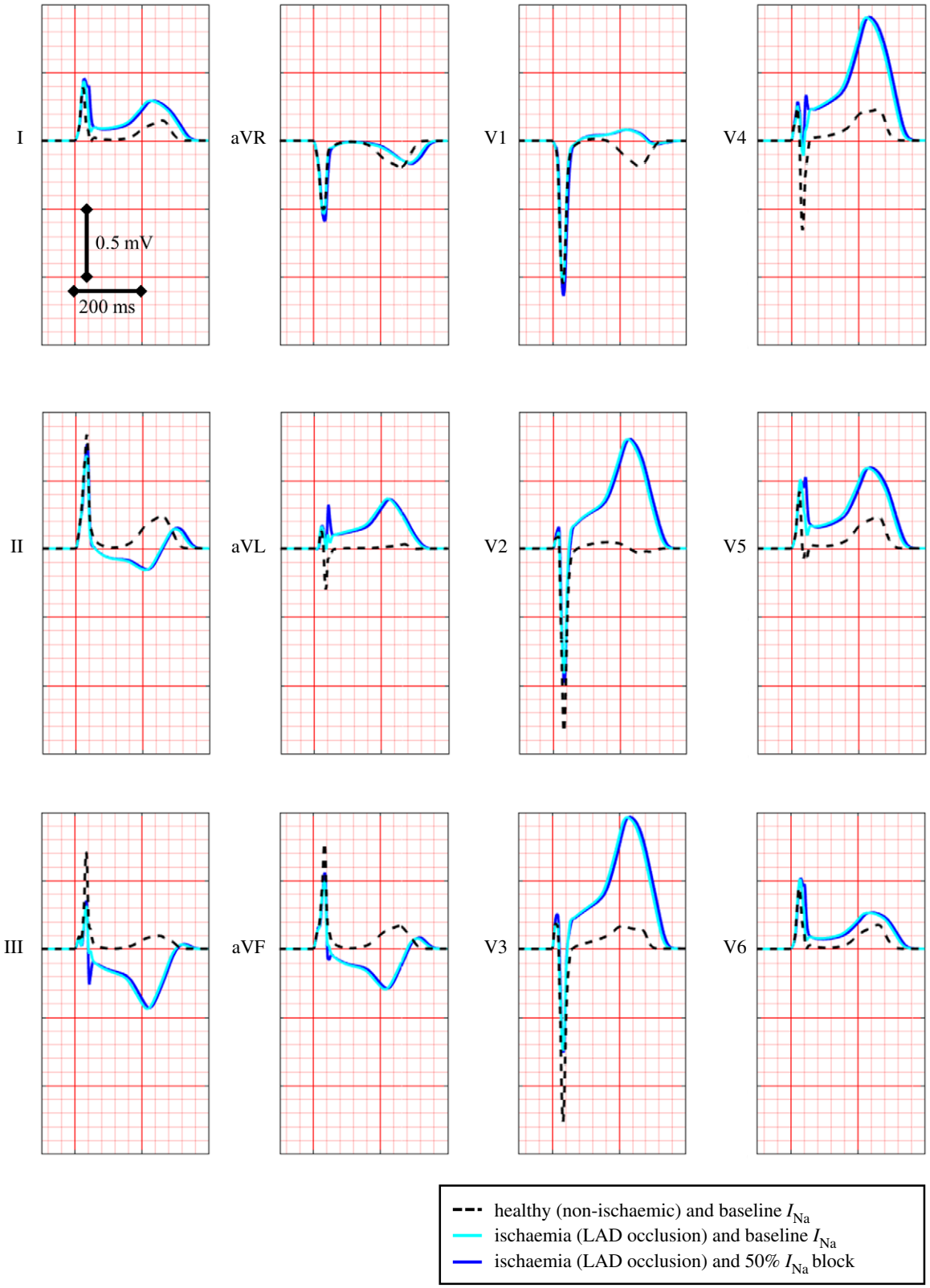

Figure 7. Simulated 12-lead ECG signal under control conditions (black dashed line), in ischaemia (light blue solid line) and ischaemia plus 50% I_{Na} block (dark blue solid line). Ischaemia leads to severe ECG changes, such as T-wave inversion in various leads (III, aVF and V1) and severe ST elevation in leads (V2–V4) in agreement with clinical data, as shown in [12]. ECG changes induced by additional 50% I_{Na} block in acute ischaemia are minor.

the high arrhythmic risk observed in patients with SCN5A mutations, and for life-threatening side effects of sodium blockers in ischaemic patients, as reported in the CAST. Under conditions of low I_{Na} availability, differences in RV versus LV thickness explain high arrhythmic risk in acute ischaemia, specifically for ectopic stimuli originating from the RV and ventricular base. The increased arrhythmic risk with low I_{Na} availability is not reflected in the ECG, which is hardly affected. Furthermore, increased I_{Na} availability was ineffective in reducing arrhythmic risk for septo-basal ectopics. The mechanisms unravelled through our simulations highlight the important role played by the asymmetric biventricular anatomy in modulating arrhythmic risk in acute regional ischaemia and its modulation by I_{Na} availability.

Data accessibility. The numerical solver CHASTE is freely available as open source at http://www.cs.ox.ac.uk/chaste/download.html.

Meshes can be found at https://doi.org/10.5287/bodleian:9RxJPo9po; models and scripts to simulate simulation outputs are provided as electronic supplementary material.

Authors' contributions. All authors conceived and designed the study. H.M.-N. performed the ventricular/torso simulations and analysed the data. X.Z. performed the ventricular fibre simulations and analysed the data. H.M.-N. prepared the figures. H.M.-N., X.Z. and B.R. drafted the manuscript. All authors interpreted the results; all authors edited and revised the manuscript.

Competing interests. The authors declare no competing interests.

Funding. This work was supported by a Wellcome Trust Fellowship in Basic Biomedical Sciences to B.R. (100246/Z/12/Z and 214290/Z/18/Z), a doctoral scholarship by the Computer Science Department in the University of Oxford to H.M.-N. and a British Heart Foundation (BHF) Intermediate Basic Science Fellowship to A.B.-O. (FS/17/22/32644). The authors also acknowledge additional support from the CompBioMed Centre of Excellence in Computational Biomedicine (European Commission Horizon 2020 research and innovation programme, grant agreement nos. 675451 and 823712), an NC3Rs Infrastructure for Impact Award (NC/P001076/1) and the Oxford BHF Centre of Research Excellence (RE/13/1/30181). This work made use of the facilities of the UK National Supercomputing Service (Archer Leadership Award e462, Archer RAP Award 00180) and a PRACE project (2017174226).

References

1. Carmeliet E. 1999 Cardiac ionic currents and acute ischemia: from channels to arrhythmias. *Physiol. Rev.* **79**, 917–1017. (doi:10.1152/physrev.1999.79.3.917)
2. Anderson JL, Platia EV, Hallstrom A, Henthorn RW, Buckingham TA, Carlson MD, Carson PE. 1994 Interaction of baseline characteristics with the hazard of encainide, flecainide, and moricizine therapy in patients with myocardial infarction. A possible explanation for increased mortality in the Cardiac Arrhythmia Suppression Trial (CAST). *Circulation* **90**, 2843–2852. (doi:10.1161/01.CIR.90.6.2843)
3. Greenberg HM, Dwyer EM, Hochman JS, Steinberg JS, Echt DS, Peters RW. 1995 Interaction of ischaemia and encainide/flecainide treatment: a proposed mechanism for the increased mortality in CAST I. *Br. Heart J.* **74**, 631–635. (doi:10.1136/hrt.74.6.631)
4. Hu D *et al.* 2007 Novel mutation in the SCN5A gene associated with arrhythmic storm developing during acute myocardial infarction. *Heart Rhythm Off. J. Heart Rhythm Soc.* **4**, 1072–1080. (doi:10.1016/j.hrthm.2007.03.040)
5. Kujime S *et al.* 2017 Outcomes of Brugada syndrome patients with coronary artery vasospasm. *Intern. Med.* **56**, 129–135. (doi:10.2169/internalmedicine.56.7307)
6. Arevalo HJ, Vadakkumpadan F, Guallar E, Jebb A, Malamas P, Wu KC, Trayanova NA. 2016 Arrhythmia risk stratification of patients after myocardial infarction using personalized heart models. *Nat. Commun.* **7**, ncomms11437. (doi:10.1038/ncomms11437)
7. Loewe A, Poremba E, Oesterlein T, Luik A, Schmitt C, Seemann G, Dössel O. 2019 Patient-specific identification of atrial flutter vulnerability—a computational approach to reveal latent reentry pathways. *Front. Physiol.* **9**, 1910. (doi:10.3389/fphys.2018.01910)
8. Moreno JD *et al.* 2011 A computational model to predict the effects of class I anti-arrhythmic drugs on ventricular rhythms. *Sci. Transl. Med.* **3**, 98ra83. (doi:10.1126/scitranslmed.3002588)
9. Passini E, Britton OJ, Lu HR, Rohrbacher J, Hermans AN, Gallacher DJ, Greig RJH, Bueno-Orovio A, Rodriguez B. 2017 Human in silico drug trials demonstrate higher accuracy than animal models in predicting clinical pro-arrhythmic cardiotoxicity. *Front. Physiol.* **8**, 668. (doi:10.3389/fphys.2017.00668)
10. Vandersickel N, Watanabe M, Tao Q, Fostier J, Zeppenfeld K, Panfilov AV. 2018 Dynamical anchoring of distant arrhythmia sources by fibrotic regions via restructuring of the activation pattern. *PLoS Comput. Biol.* **14**, e1006637. (doi:10.1371/journal.pcbi.1006637)
11. Loewe A, Schulze WHW, Jiang Y, Wilhelms M, Luik A, Dössel O, Seemann G. 2015 ECG-based detection of early myocardial ischemia in a computational model: impact of additional electrodes, optimal placement, and a new feature for ST deviation. *BioMed Res. Int.* **2015**, 530352. (doi:10.1155/2015/530352)
12. Martinez-Navarro H, Mincholé A, Bueno-Orovio A, Rodriguez B. 2019 High arrhythmic risk in antero-septal acute myocardial ischemia is explained by increased transmural reentry occurrence. *Sci. Rep.* **9**, 16803. (doi:10.1038/s41598-019-53221-2)
13. Wilhelms M, Dossel O, Seemann G. 2011 In silico investigation of electrically silent acute cardiac ischemia in the human ventricles. *IEEE Trans. Biomed. Eng.* **58**, 2961–2964. (doi:10.1109/TBME.2011.2159381)
14. Boyle PM, Park CJ, Arevalo HJ, Vigmond EJ, Trayanova NA. 2014 Sodium current reduction unmasks a structure-dependent substrate for arrhythmogenesis in the normal ventricles. *PLoS ONE* **9**, e86947. (doi:10.1371/journal.pone.0086947)
15. Moreno JD, Lewis TJ, Clancy CE. 2016 Parameterization for in-silico modeling of ion channel interactions with drugs. *PLoS ONE* **11**, e0150761. (doi:10.1371/journal.pone.0150761)
16. O'Hara T, Virág L, Varró A, Rudy Y. 2011 Simulation of the undiseased human cardiac ventricular action potential: model formulation and experimental validation. *PLoS Comput. Biol.* **7**, e1002061. (doi:10.1371/journal.pcbi.1002061)
17. Dutta S, Mincholé A, Quinn TA, Rodriguez B. 2017 Electrophysiological properties of computational human ventricular cell action potential models under acute ischemic conditions. *Prog. Biophys. Mol. Biol.* **129**, 40–52. (doi:10.1016/j.pbiomolbio.2017.02.007)
18. Curtis MJ. 1998 Characterisation, utilisation and clinical relevance of isolated perfused heart models of ischaemia-induced ventricular fibrillation. *Cardiovasc. Res.* **39**, 194–215. (doi:10.1016/S0008-6363(98)00083-2)
19. Lindsey ML *et al.* 2018 Guidelines for experimental models of myocardial ischemia and infarction. *Am. J. Physiol. Heart Circ. Physiol.* **314**, H812–H838. (doi:10.1152/ajpheart.00335.2017)
20. Dutta S, Mincholé A, Zacur E, Quinn TA, Taggart P, Rodriguez B. 2016 Early afterdepolarizations promote transmural reentry in ischemic human ventricles with reduced repolarization reserve. *Prog. Biophys. Mol. Biol.* **120**, 236–248. (doi:10.1016/j.pbiomolbio.2016.01.008)
21. Coronel R, Wilms-Schopman FJ, Opthof T, van Capelle FJ, Janse MJ. 1991 Injury current and gradients of diastolic stimulation threshold, TQ potential, and extracellular potassium concentration during acute regional ischemia in the isolated perfused pig heart. *Circ. Res.* **68**, 1241–1249. (doi:10.1161/01.RES.68.5.1241)
22. Janse MJ, van Capelle FJ, Morsink H, Kléber AG, Wilms-Schopman F, Cardinal R, D'alnoncourt CN, Durrer D. 1980 Flow of 'injury' current and patterns of excitation during early ventricular arrhythmias in acute regional myocardial ischemia in isolated porcine and canine hearts. Evidence for two different arrhythmogenic mechanisms. *Circ. Res.* **47**, 151–165. (doi:10.1161/01.RES.47.2.151)
23. Wilensky RL, Tranum-Jensen J, Coronel R, Wilde AA, Fiolet JW, Janse MJ. 1986 The subendocardial border zone during acute ischemia of the rabbit heart: an electrophysiologic, metabolic, and morphologic correlative study. *Circulation* **74**, 1137–1146. (doi:10.1161/01.CIR.74.5.1137)
24. Moréna H, Janse MJ, Fiolet JW, Krieger WJ, Crijns H, Durrer D. 1980 Comparison of the effects of regional ischemia, hypoxia, hyperkalemia, and acidosis on intracellular and extracellular potentials and metabolism in the isolated porcine heart. *Circ. Res.* **46**, 634–646. (doi:10.1161/01.RES.46.5.634)
25. Vermeulen JT, Tan HL, Rademaker H, Schumacher CA, Loh P, Opthof T, Coronel R, Janse MJ. 1996 Electrophysiologic and extracellular ionic changes during acute ischemia in failing and normal rabbit myocardium. *J. Mol. Cell. Cardiol.* **28**, 123–131. (doi:10.1006/jmcc.1996.0012)
26. Michailova A, Saucerman J, Belik ME, McCulloch AD. 2005 Modeling regulation of cardiac KATP and L-type Ca^{2+} currents by ATP, ADP, and Mg^{2+}. *Biophys. J.* **88**, 2234–2249. (doi:10.1529/biophysj.104.046284)

27. Ferrero JM, Trénor B, Rodríguez B, Sáiz J. 2003 Electrical activity and reentry during acute regional myocardial ischemia: insights from simulations. *Int. J. Bifurc. Chaos* **13**, 3703–3715. (doi:10.1142/S0218127403008806)
28. Rodríguez B, Trayanova N, Noble D. 2006 Modeling cardiac ischemia. *Ann. NY Acad. Sci.* **1080**, 395–414. (doi:10.1196/annals.1380.029)
29. Tice BM, Rodríguez B, Eason J, Trayanova N. 2007 Mechanistic investigation into the arrhythmogenic role of transmural heterogeneities in regional ischaemia phase 1A. *Europace* **9**(Suppl. 6), vi46–vi58. (doi:10.1093/europace/eum204)
30. Trénor B, Ferrero JM, Rodríguez B, Montilla F. 2005 Effects of pinacidil on reentrant arrhythmias generated during acute regional ischemia: a simulation study. *Ann. Biomed. Eng.* **33**, 897–906. (doi:10.1007/s10439-005-3554-4)
31. Pathmanathan P, Bernabeu MO, Bordas R, Cooper J, Garny A, Pitt-Francis JM, Whiteley JP, Gavaghan DJ. 2010 A numerical guide to the solution of the bi-domain equations of cardiac electrophysiology. *Prog. Biophys. Mol. Biol.* **102**, 136–155. (doi:10.1016/j.pbiomolbio.2010.05.006)
32. Pitt-Francis J *et al.* 2008 Chaste: using agile programming techniques to develop computational biology software. *Phil. Trans. R. Soc. A* **366**, 3111–3136. (doi:10.1098/rsta.2008.0096)
33. Cardone-Noott L, Bueno-Orovio A, Mincholé A, Zemzemi N, Rodriguez B. 2016 Human ventricular activation sequence and the simulation of the electrocardiographic QRS complex and its variability in healthy and intraventricular block conditions. *Europace* **18**(Suppl 4), iv4–iv15. (doi:10.1093/europace/euw346)
34. Streeter DD, Spotnitz HM, Patel DP, Ross J, Sonnenblick EH. 1969 Fiber orientation in the canine left ventricle during diastole and systole. *Circ. Res.* **24**, 339–347. (doi:10.1161/01.RES.24.3.339)
35. Szentadrassy N *et al.* 2005 Apico-basal inhomogeneity in distribution of ion channels in canine and human ventricular myocardium. *Cardiovasc. Res.* **65**, 851–860. (doi:10.1016/j.cardiores.2004.11.022)
36. Weiss DL, Seemann G, Keller DUJ, Farina D, Sachse FB, Dossel O. 2007 Modeling of heterogeneous electrophysiology in the human heart with respect to ECG genesis. In *2007 Computers in Cardiology, Durham, NC, USA, 30 September–3 October 2007*, pp. 49–52. (doi:10.1109/CIC.2007.4745418)
37. Durrer D, Dam RTV, Freud GE, Janse MJ, Meijler FL, Arzbaecher RC. 1970 Total excitation of the isolated human heart. *Circulation* **41**, 899–912. (doi:10.1161/01.CIR.41.6.899)
38. Coronel R, Wilms-Schopman FJ, Dekker LR, Janse MJ. 1995 Heterogeneities in [K+]o and TQ potential and the inducibility of ventricular fibrillation during acute regional ischemia in the isolated perfused porcine heart. *Circulation* **92**, 120–129. (doi:10.1161/01.CIR.92.1.120)
39. de Vries LJ, Martirosyan M, van Domburg RT, Wijchers SA, Géczy T, Szili-Torok T. 2018 Coupling interval variability of premature ventricular contractions in patients with different underlying pathology: an insight into the arrhythmia mechanism. *J. Interv. Card. Electrophysiol.* **51**, 25–33. (doi:10.1007/s10840-017-0309-8)
40. Liu M, Yang K, Dudley S. 2014 Cardiac sodium channel mutations: why so many phenotypes? *Nat. Rev. Cardiol.* **11**, 607–615. (doi:10.1038/nrcardio.2014.85)
41. Brennan T, Fink M, Rodriguez B. 2009 Multiscale modelling of drug-induced effects on cardiac electrophysiological activity. *Eur. J. Pharm. Sci.* **36**, 62–77. (doi:10.1016/j.ejps.2008.09.013)
42. Crumb WJ, Vicente J, Johannesen L, Strauss DG. 2016 An evaluation of 30 clinical drugs against the comprehensive in vitro proarrhythmia assay (CiPA) proposed ion channel panel. *J. Pharmacol. Toxicol. Methods* **81**, 251–262. (doi:10.1016/j.vascn.2016.03.009)
43. Aliot E, Capucci A, Crijns HJ, Goette A, Tamargo J. 2011 Twenty-five years in the making: flecainide is safe and effective for the management of atrial fibrillation. *Europace* **13**, 161–173. (doi:10.1093/europace/euq382)
44. Andrikopoulos GK, Pastromas S, Tzeis S. 2015 Flecainide: current status and perspectives in arrhythmia management. *World J. Cardiol.* **7**, 76–85. (doi:10.4330/wjc.v7.i2.76)
45. Lau DH *et al.* 2009 Epicardial border zone overexpression of skeletal muscle sodium channel SkM1 normalizes activation, preserves conduction, and suppresses ventricular arrhythmia: an in silico, in vivo, in vitro study. *Circulation* **119**, 19–27. (doi:10.1161/CIRCULATIONAHA.108.809301)
46. Laguna P, Sörnmo L. 2014 The STAFF III ECG database and its significance for methodological development and evaluation. *J. Electrocardiol.* **47**, 408–417. (doi:10.1016/j.jelectrocard.2014.04.018)
47. Echt DS *et al.* 1991 Mortality and morbidity in patients receiving encainide, flecainide, or placebo. The Cardiac Arrhythmia Suppression Trial. *N. Engl. J. Med.* **324**, 781–788. (doi:10.1056/NEJM199103213241201)
48. Kucera JP, Rudy Y. 2001 Mechanistic insights into very slow conduction in branching cardiac tissue. *Circ. Res.* **89**, 799–806. [cited 19 November 2019]. (doi:10.1161/hh2101.098442)
49. Rohr S. 2004 Role of gap junctions in the propagation of the cardiac action potential. *Cardiovasc. Res.* **62**, 309–322. (doi:10.1016/j.cardiores.2003.11.035)
50. Ciaccio EJ *et al.* 2007 Model of reentrant ventricular tachycardia based on infarct border zone geometry predicts reentrant circuit features as determined by activation mapping. *Heart Rhythm* **4**, 1034–1045. (doi:10.1016/j.hrthm.2007.04.015)
51. Ciaccio EJ, Coromilas J, Ashikaga H, Cervantes DO, Wit AL, Peters NS, Mcveigh ER, Garan H. 2015 Model of unidirectional block formation leading to reentrant ventricular tachycardia in the infarct border zone of postinfarction canine hearts. *Comput. Biol. Med.* **62**, 254–263. (doi:10.1016/j.compbiomed.2015.04.032)
52. Letsas KP, Asvestas D, Vlachos K, Karlis D, Korantzopoulos P, Efremidis M, Sideris A. 2014 Electrocardiographic characteristics of premature ventricular contractions in subjects with type 1 pattern of Brugada syndrome. *J. Electrocardiol.* **47**, 351–355. (doi:10.1016/j.jelectrocard.2014.02.012)
53. Morita H *et al.* 2003 Site-specific arrhythmogenesis in patients with Brugada syndrome. *J. Cardiovasc. Electrophysiol.* **14**, 373–379. (doi:10.1046/j.1540-8167.2003.02365.x)
54. Brugada R, Brugada J, Antzelevitch C, Kirsch GE, Potenza D, Towbin JA, Brugada P. 2000 Sodium channel blockers identify risk for sudden death in patients with ST-segment elevation and right bundle branch block but structurally normal hearts. *Circulation* **101**, 510–515. (doi:10.1161/01.CIR.101.5.510)
55. Ellinor PT, Nam EG, Shea MA, Milan DJ, Ruskin JN, MacRae CA. 2008 Cardiac sodium channel mutation in atrial fibrillation. *Heart Rhythm* **5**, 99–105. (doi:10.1016/j.hrthm.2007.09.015)
56. Li Q *et al.* 2009 Gain-of-function mutation of Nav1.5 in atrial fibrillation enhances cellular excitability and lowers the threshold for action potential firing. *Biochem. Biophys. Res. Commun.* **380**, 132–137. (doi:10.1016/j.bbrc.2009.01.052)
57. Makiyama T *et al.* 2008 A novel SCN5A gain-of-function mutation M1875T associated with familial atrial fibrillation. *J. Am. Coll. Cardiol.* **52**, 1326–1334. (doi:10.1016/j.jacc.2008.07.013)
58. Bueno-Orovio A, Cherry EM, Evans SJ, Fenton FH. 2015 Basis for the induction of tissue-level phase-2 reentry as a repolarization disorder in the Brugada syndrome. *BioMed Res. Int.* **2015**, 197586. (doi:10.1155/2015/197586)
59. Meregalli PG, Wilde AAM, Tan HL. 2005 Pathophysiological mechanisms of Brugada syndrome: depolarization disorder, repolarization disorder, or more? *Cardiovasc. Res.* **67**, 367–378. (doi:10.1016/j.cardiores.2005.03.005)
60. Zhang J *et al.* 2015 Cardiac electrophysiological substrate underlying the ECG phenotype and electrogram abnormalities in Brugada syndrome patients. *Circulation* **131**, 1950–1959. (doi:10.1161/CIRCULATIONAHA.114.013698)
61. Deschênes I, Baroudi G, Berthet M, Barde I, Chalvidan T, Denjoy I, Guicheney P, Chahine M. 2000 Electrophysiological characterization of SCN5A mutations causing long QT (E1784 K) and Brugada (R1512 W and R1432G) syndromes. *Cardiovasc. Res.* **46**, 55–65. (doi:10.1016/S0008-6363(00)00006-7)
62. Shirai N *et al.* 2002 A mutant cardiac sodium channel with multiple biophysical defects associated with overlapping clinical features of Brugada syndrome and cardiac conduction disease. *Cardiovasc. Res.* **53**, 348–354. (doi:10.1016/S0008-6363(01)00494-1)
63. Tan B-H, Valdivia CR, Song C, Makielski JC. 2006 Partial expression defect for the SCN5A missense mutation G1406R depends on splice variant background Q1077 and rescue by mexiletine. *Am. J. Physiol. Heart Circ. Physiol.* **291**, H1822–H1828. (doi:10.1152/ajpheart.00101.2006)